

Article

# Properties of Biochar from Anaerobically Digested Food Waste and Its Potential Use in Phosphorus Recovery and Soil Amendment

Shakib Alghashm <sup>1</sup>, Shiying Qian <sup>1</sup>, Yinfeng Hua <sup>2</sup>, Jian Wu <sup>2</sup>, Haitao Zhang <sup>2</sup>, Weihua Chen <sup>2</sup> and Guoqing Shen <sup>1,\*</sup>

<sup>1</sup> School of Agriculture and Biology, Shanghai Jiao Tong University, 800 Dongchuan Road, Shanghai 200240, China; shakibalghashm@gmail.com (S.A.); qsy0901@sjtu.edu.cn (S.Q.)

<sup>2</sup> Shanghai Liming Resources Reuse Co. Ltd., Shanghai 201209, China; Huayf2015@126.com (Y.H.); woojan@aliyun.com (J.W.); diabc@126.com (H.Z.); cwh62500@163.com (W.C.)

\* Correspondence: gqsh@sjtu.edu.cn; Tel.: +86-21-342-061-43

Received: 14 November 2018; Accepted: 5 December 2018; Published: 10 December 2018



**Abstract:** The disposal of a large amount of biogas residue from anaerobically digested food waste is a burden for biogas production. The aim of this work was to investigate biogas residue as a potential feedstock, by preparing biochar at a broad pyrolysis temperature range of 400–900 °C. The properties required for phosphorus recovery and soil amendment application were evaluated. Biogas residue collected from an urban food waste treatment plant was pyrolyzed in a laboratory scale reactor. It was found that by increasing the pyrolysis temperature, the yield of biochar decreased and the pH, electrical conductivity and Brunauer–Emmett–Teller surface area increased. The amount of phosphorus adsorbed onto the biogas residue-derived biochar (BRB) at 900 °C was larger than that of other kinds of biochar. The kinetics of phosphorus (P) adsorption on BRB could be described by the pseudo-second-order equation. The pot experiments showed that the resulting biochar is beneficial for the growth of cabbage. Overall, turning solid residue from the anaerobic digestion of food waste for biogas production into biochar shows good prospects as a means of solving the disposal problem, while creating new markets for food waste biogas residue.

**Keywords:** pyrolysis temperature; biogas residue; adsorption; pseudo-second-order equation

---

## 1. Introduction

With increasing global economic development and urban populations, food waste is largely produced by the ever-growing demand from hotels, canteens, hypermarkets and companies [1]. Significant pollution in the environment has been caused by the excessive discharge of huge amounts of food waste. Traditional disposal methods include landfilling, incineration and composting. However, huge financial costs are required in order to dispose of food waste without negatively affecting the environment. Many solutions and practices have been proposed, and they are often implemented in order to “keep food out of landfills”, thus reducing food waste at the source [2–5]. Gupta et al. [6] reported that the conversion of food waste into biogas is considered as an effective strategy to solve the food waste management problem. Anaerobic digestion has been found to be better than traditional disposal methods, because it offers dual benefits: First, it promises the safe disposal of waste, and second, it is a renewable source for biogas production. However, biogas residue (BR) produced during the anaerobic digestion of food waste may remain a burden. It is necessary to find an effective strategy for the safe disposal of biogas residue. Recently, the use of residue from biogas production for soil amendment has been increasingly investigated due to the high organic content in biogas residue.

However, its application for soil amendment can be limited, due to the presence of pathogens/harmful elements in the residue [7]. To overcome this problem, converting biogas residue waste to biochar using pyrolysis can be an effective way to reduce the level of harmful pathogens. Following this process, biogas residue can then be used as a biofertilizer [7–12]. However, only a few studies have reported the use of biogas residue from food waste as a means of utilizing biochar. Yet, the utilization of biochar, being a novel approach, could benefit both waste management and economic development. Therefore, it is necessary to research this process to develop a fuller understanding.

Thermochemical conversion of digestate results in the formation of a solid material known as biochar. This conversion happens in an oxygen-limited environment [13]. Several studies have reported on carbon sequestration and soil amelioration applications. There has also been some research suggesting that biochar is cost-effective as an adsorbent, due to its ability to store chemical compounds [14]. However, the yield and physicochemical characteristics of biochar can vary widely, depending on pyrolysis conditions, which are some of the most influential factors. Qin et al. [15] reported the characteristics of biochar derived from rice husks in a wide pyrolysis temperature range. The findings illustrated a U-shaped relationship between the biochar pyrolysis temperature and efficiency. It is necessary to gain a further understanding of the physicochemical parameters of biochar derived from various sources for its safe disposal. Some studies have reported on biochar production from anaerobically digested biomass, including sugarcane bagasse [16], sugar beet tailings [14] and pig manure [17]. There are very few studies on the characteristics of biochar from anaerobically digested food waste for biogas production, and this needs further investigation.

A deficiency in phosphorus (P) resources and P wastewater pollution are considered serious problems worldwide [18]. In recent years, the application of biochar as an environmentally friendly adsorbent has attracted interest in P recovery studies. Chen et al. [19] documented that magnetic biochars made from iron-treated orange peel powder had a P adsorption capacity of  $1.2 \text{ mg}\cdot\text{g}^{-1}$ . Hammer et al. [20] stated that wood pellet biochars had a P adsorption ability of  $7.7161 \text{ mg}\cdot\text{g}^{-1}$ . Given that shortages in phosphorus can be addressed by biochar, the investigation of using biochar from biogas residue has huge potential. Interestingly, the application of biochar in agriculture can be an effective way to enhance soil fertility, as it may contain multiple minerals that are required for soil enrichment. Chen et al. [21] reported the addition of biochar produced from cow dung to agricultural soil, and confirmed that P-laden biochar not only increased the germination rate, but also promoted plant growth. However, to the best of our knowledge, only limited information is available on the utilization of phosphorus from biochar produced from food waste-derived biomass.

In this study, biochars were made from anaerobically digested food waste biogas residues through slow pyrolysis from  $400^\circ\text{C}$  to  $900^\circ\text{C}$ . The physicochemical properties of the biochar that was produced were characterized, and a simple adsorption experiment was conducted as a preliminary assessment of its phosphate adsorption ability. Our objectives were to: (1) Determine whether anaerobically digested food waste biogas can be efficiently used as feedstock for biochar, (2) investigate the influence of pyrolysis temperature on the physicochemical properties of biochar from anaerobically digested food waste, and (3) assess the potential use of biochar in phosphorus recovery and soil amendment.

## 2. Materials and Methods

### 2.1. Biochar Production

Biogas residue (BR) from anaerobic food waste digestion was obtained from an organic solid waste treatment plant located at Pudong Liming Eco-Industrial Park in Shanghai, China. The waste was left to dry at ambient air temperature under the sun. After that, the aggregates were softly crushed and the particles were passed through a 0.4 mm sieve to ensure a homogeneous particle size. The moisture content in the feedstock samples was 7.49%. The feedstock samples were pyrolyzed at 400 to  $900^\circ\text{C}$ , using a pyrolysis time of 2 h maintained under oxygen-limited conditions in a muffle furnace (Shanghai Yi Zhong Inc., Shanghai, China).

## 2.2. Fourier Transform Infrared (FTIR) Analysis

Fourier transform infrared (FTIR) spectra of the samples (biochar) were obtained through diffuse reflectance infrared 150 Fourier transform spectroscopy. Briefly, the samples were ground to 0.1 mm, and 0.5 g was placed for analysis in the FTIR sampling window (Nicolet 5700 FTIR-OMNI Sampler Nexus). A KBr beam splitter was used to obtain the spectra (256 scans). The range was set to 4500 to 650  $\text{cm}^{-1}$  (aperture size: 34 cm). OMNIC v7.1 software with Happ–Genzel apodization was used to analyze the measured transmission.

## 2.3. Pyrolysis Yield and Volatile Matter

The ratio of the sample biochar weight to the dry weight of the residues was determined as the pyrolysis yield. The percentage of volatile matter was determined by pulverizing 2 g of biochar sample in a crucible, placing it at a temperature of 950  $^{\circ}\text{C}$  for 6 min and then weighing it. The volatile matter was then calculated using following equation:

$$\text{Volatile matter (\%)} = [(B - C)/B] \times 100 \quad (1)$$

where  $B$  and  $C$  are grams of sample after drying at 105  $^{\circ}\text{C}$  and 950  $^{\circ}\text{C}$ , respectively.

## 2.4. pH, Electrical Conductivity (EC) Values, and Elemental Composition

A 1 g sample of dry BR or BR-derived biochar was suspended in 10 mL of deionized water and put in a shaker for 30 min. The pH and electrical conductivity (EC) of the suspension were measured using a digital pH meter (Sartorius PB-10, Bohemia, NY, USA) and a conductivity meter (DDS-307 A, Shanghai, China). The elemental amounts of C, H, N, S, and O were determined by an elemental analyzer (vario EL cube; Elementar Co., Langenselbold, Germany, 2013). The sample was dropped into a hot furnace (1150  $^{\circ}\text{C}$ ), and through the combustion of oxygen, the reduction temperature was 850  $^{\circ}\text{C}$ , with copper reduction [22].

## 2.5. Surface Area ( $S_{\text{BET}}$ )

The BR and BR-derived parameters were determined for porous structures at low-temperature (77.4 K)  $\text{N}_2$  adsorption-desorption isotherms, which were obtained from an ASAP 2420 surface area and a porosity analyzer (Micromeritics, Norcross, GA, USA). From the adsorption branch data, using the linear form of the Brunauer–Emmett–Teller (BET) equation, the specific surface area ( $S_{\text{BET}}$ ) was calculated.

## 2.6. Phosphorus Adsorption

The P adsorption capacity of the biochar sample was found as described by Chen et al. (2018). In brief, the sample (0.5 g) was mixed with a phosphate solution (50 mL, 200–600  $\text{mg L}^{-1}$ ) in flasks and sealed and kept in an orbital shaker at 120 rpm for 24 h at room temperature (RT). The samples were then filtered and the concentration of adsorbed phosphorus was determined. The results were consistent with previously reported findings [23,24], suggesting that 24 h of incubation was sufficient, and that the P adsorption capacity was determined using the following equation [25]:

$$Y = \frac{(C_o - C_e)V}{M} \quad (2)$$

where  $Y$  is the P adsorption capacity ( $\text{mg}\cdot\text{g}^{-1}$ );  $V$  is the volume of P solution (L);  $C_o$  and  $C_e$  are the initial and equilibrium phosphate concentrations in aqueous solution, respectively ( $\text{mg}\cdot\text{L}^{-1}$ ); and  $M$  is the mass of the biochar sample used (g). The P concentrations in aqueous solution were measured using the automated molybdenum blue colorimetric method [26].

## 2.7. Adsorption Kinetic Analysis

The adsorption kinetics analysis was carried out using two well-known kinetic models: The pseudo-first-order model and the pseudo-second-order model, which are shown in Equations (3) and (4), respectively:

$$Q_t = Q_e(1 - \exp(-k_1 t)) \quad (3)$$

$$Q_t = Q_e k_2 t / (1 + Q_m k_2 t) \quad (4)$$

where  $t$  denotes the contact time (min);  $Q_e$  and  $Q_t$  denote the amount of  $P$  ( $\text{mg} \cdot \text{g}^{-1}$ ) adsorbed at equilibrium and at a given time, respectively; and  $k_1$  ( $\text{min}^{-1}$ ) and  $k_2$  ( $\text{g} \cdot (\text{mg} \cdot \text{min})^{-1}$ ) are the rate constants of the pseudo-first-order and pseudo-second-order kinetics models, respectively.

## 2.8. Pot Experiment

The pot experiment was done as a set of 7 experiments in a greenhouse in triplicate as a randomized trial. Each pot contained 750 g of soil and the biochar amendment rate was 1%  $w/w$  dry weight. Cabbage seeds (*Brassica chinensis* L.) were sprinkled on moistened filter paper in a petri dish. On day 7, one plant per pot was sown with the germinated seeds. All pots were watered daily under greenhouse conditions. The weights of the fresh biomass, plant height and leaf area were determined by harvesting the plant samples after 45 days.

## 3. Results and Discussion

### 3.1. Pyrolysis Yield

The yield of biochar is a co-product of fast pyrolysis with lignocellulosic biomass. Table 1 shows that the percentage of pyrolysis yield declined with increased temperature, where there was 70.35% of the real mass at 400 °C to 43.65% at 900 °C. The content of volatile matter also decreased, from 55.36% to 4.49%. In general, the thermal deterioration of biomass was present at a lower pyrolysis temperature. Nonetheless, the pyrolytic volatiles split into low-set atomic weight organics and gases, instead of biochar, as pyrolysis temperature increased [27]. This diminishing direction of biochar as pyrolysis increased was in agreement with studies on the pyrolytic properties of woody biomass [28]. Based on the results of research on various materials, a reduction in yield can be due to the loss of chemically bound moisture, the decomposition of organic substances and the dehydration of hydroxyl groups, or at higher temperatures it can be induced by the buildup of aromatic structures, with damage to large amounts of CO<sub>2</sub>, CO, H<sub>2</sub>O, and H<sub>2</sub> [8].

**Table 1.** Main properties of biogas residue and biochars at various temperatures.

| Biogas Residue   | Biogas Residue-Derived Biochar |              |              |              |              |              |
|------------------|--------------------------------|--------------|--------------|--------------|--------------|--------------|
|                  | 400 °C                         | 500 °C       | 600 °C       | 700 °C       | 800 °C       | 900 °C       |
| PY               | 70.35 ± 0.08                   | 68.25 ± 0.13 | 66.02 ± 0.01 | 64.38 ± 0.62 | 56.33 ± 0.46 | 43.65 ± 0.08 |
| VM               | 55.36 ± 0.07                   | 40.67 ± 0.16 | 34.90 ± 0.09 | 33.31 ± 0.18 | 30.52 ± 0.04 | 20.68 ± 0.05 |
| pH               | 7.95 ± 0.03                    | 9.19 ± 0.08  | 9.28 ± 0.02  | 10.60 ± 0.25 | 11.56 ± 0.20 | 12.51 ± 0.05 |
| EC               | 3.88 ± 0.39                    | 2.23 ± 0.10  | 3.05 ± 0.04  | 3.17 ± 0.04  | 3.20 ± 0.01  | 12.66 ± 0.05 |
| S <sub>BET</sub> | 8.48                           | 17.91        | 19.05        | 21.68        | 25.96        | 29.42        |
|                  |                                |              |              |              |              | 66.15        |

PY, pyrolytic yield (%); VM, volatile matter (%); EC, electrical conductivity ( $\text{mS} \cdot \text{cm}^{-1}$ ); S<sub>BET</sub>, specific surface area ( $\text{m}^2 \cdot \text{g}^{-1}$ ).

### 3.2. pH Values and Electrical Conductivity (EC)

Pyrolyzing biochars increased their pH and produced alkaline biochars. The pH of the biochar increased remarkably compared to the pH of the raw feedstock (Table 1). The pH of the feedstock biogas residue sample was 7.95, and the pH of biochar increased from 9.19 to 12.52 with pyrolysis temperature ranging from 400 °C to 900 °C. Cao et al. [29] reported that when the pyrolysis temperature was

>350 °C, cellulose, hemicellulose and lignin started to become ash, and alkali salts began to separate from the organic materials, increasing the biochar pH. Such high pH values were similar to those in biochars generated from most types of biomass, and the high pH was due to an assemblage of Ca, Mg, and K from the biogas residues during pyrolysis. The higher pH of biochars may allow them to amend and neutralize soil acidity and will also be likely to adsorb positively charged ions. The electrical conductivity (EC) value reflected the degree of salinity in the biochar. The EC values in the samples of biochar produced at 400, 500, 600 and 700 °C, respectively, were 2.23, 3.05, 3.17, and 3.20 mS·cm<sup>-1</sup>. However, these values sharply increased with a pyrolysis temperature of 800 and 900 °C and amounted to values of 12.66 and 11.50 mS·cm<sup>-1</sup>, respectively (Table 1). These results indicate that biochar produced at a high pyrolysis temperature (especially at 800 and 900 °C), when applied to the soil, may increase soil salinity and subsequently have undesirable effects on plant growth. The effects of high salinity on plant development due to the low osmotic potential of the soil solution, waterlogging, disturbance of ions and nutrient imbalance during stress are well known [30,31].

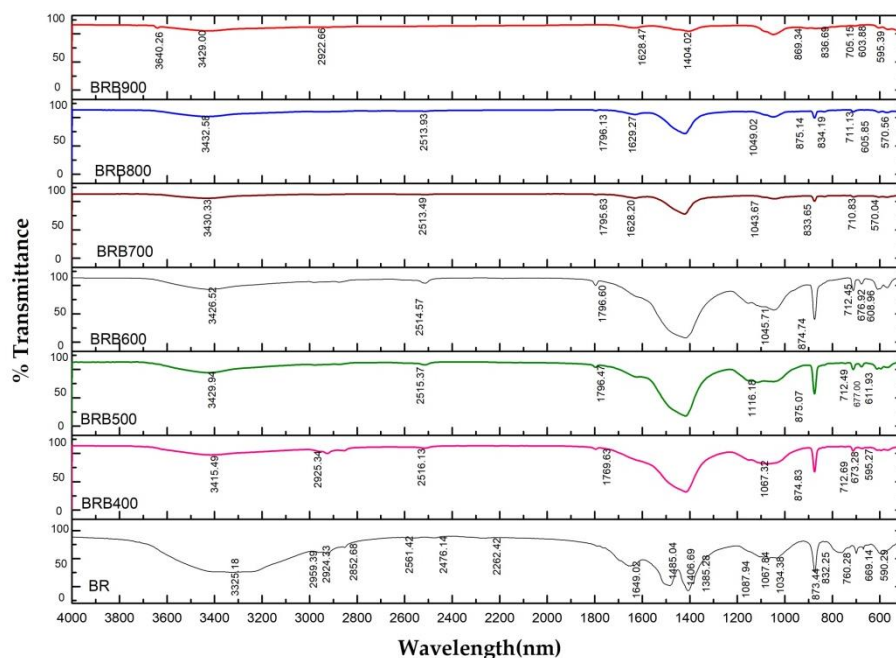
### 3.3. Surface Properties

The Brunauer–Emmett–Teller (BET) surface area of the biochar samples demonstrated substantial development throughout pyrolysis, related to their absorption capacity. Table 1 shows that the surface area of biochars ranged from 17.91 to 66.15 m<sup>2</sup>·g<sup>-1</sup> as pyrolysis temperature increased from 400 °C to 900 °C. In contrast, for biogas residue, the BET surface area of biochar was augmented eight-fold. This augmentation was due to alteration in the elemental combination at a higher temperature. The area quality and pore quantity of biochar both depend on decreasing temperature. Lower temperatures change amorphous carbon to main carbon, which does not allow pore development. Fewer pores are inhibited by aliphatic, which curtails the surface area. When the temperature increases, amorphous carbons are reduced to crystalline carbons and make more pores, which eliminate the aliphatic and volatile composition [32]. It is worth noting that the BET surface area was effectively higher from 29.42 m<sup>2</sup>·g<sup>-1</sup> to 66.15 m<sup>2</sup>·g<sup>-1</sup> when the pyrolysis temperature was raised from 800 °C to 900 °C. The pore properties (e.g., BET surface area), which increased slowly, ranged between 400 and 700 °C, thus, a critical temperature range of 800–900 °C for pyrolysis is recommended for a slightly increased surface area of biochar. According to Mukome and Parikh [33], there is a noteworthy relationship between pyrolysis temperature and the specific surface areas(SSA), which plays an important role in creating more pores at higher temperatures in most biochars. In another study, it was concluded that biochar prepared from the biogas digestate of swine manure showed an increase in the BET surface area from 700 and 800 °C. These results were in agreement with Reference [7].

### 3.4. Changes in Chemical Bond Structure with Pyrolysis Temperature

The infrared spectra of the biogas residue and biochar samples show complex chemical bond structures with a union of minerals and organic matter (Figure 1). Typically, waste from eateries and restaurants contains a lot of organic and inorganic compounds, which may give clear stretching for many groups in the fingerprint region. For instance, we are able to see O–H (3400 cm<sup>-1</sup>), C–H (2900 cm<sup>-1</sup>), C=C (1600 cm<sup>-1</sup>), and C–O (1400 cm<sup>-1</sup>) [34]. It is worth mentioning that such bands related to the functional groups were not present in the biochar. This is a clear indication that pyrolysis resulted in the conversion of most of the organic matter from the food waste (biomass) residues to inorganic matter. Of note, there are instances of the presence of residual nitrogen compounds and organic matter to a certain extent in the biochar spectrum. The FTIR spectra of the waste food from restaurants showed a high tip in lines at 3300 cm<sup>-1</sup>, which may be due to the OH vibration of the hydroxyl groups [35]. It is worth mentioning that this tip was not present in the biochar. The peaks in the spectra observed at 3000 and 2850 cm<sup>-1</sup> can be correlated with the stretching vibration of C–H bonds, most likely related to the sp<sup>3</sup> of alkanes, which was in agreement with previously published reports [36]. However, no such peak was observed in the biochar spectra, illustrating its removal during pyrolysis. The 2850 and 2660 cm<sup>-1</sup> peaks can be taken as the axial deformation majority of

the aldehydes [37]. Bands at  $1649\text{ cm}^{-1}$  can be related to the aromatic C=C vibration and the band at  $1485\text{ cm}^{-1}$  may be due to the presence of C–H from alkanes [38]. At a wavelength between  $1385$  and  $1000\text{ cm}^{-1}$ , we observed the C–O axial deformation of phenols and alcohols. Similarly, for the stretch at  $740\text{ cm}^{-1}$  and peak at  $699\text{ cm}^{-1}$ , a peak was detected due to N–H stretch, which was not seen in biochar.



### 3.5. Elemental Composition and Molecular Ratios

Table 2 shows that the elemental composition was similar for all biogas residue-derived biochars (BRBs). Total C, H, N and O was seen to decline with increasing biochar pyrolysis temperature from  $400$  to  $900\text{ }^{\circ}\text{C}$ . For example, total C and N decreased to  $19.81\%$  and  $1.41\%$ , respectively, at  $400\text{ }^{\circ}\text{C}$  to  $7.07\%$  and  $0.14\%$  at  $900\text{ }^{\circ}\text{C}$ . The decrease of carbon and nitrogen resulted from the increasing biomass combustion and organic volatilization with increasing temperature [29]. This result is consistent with findings from Agrafioti et al. [39] and Cao et al. [29]. The reduced nitrogen content of biochars may not necessarily be helpful to crops, since N mostly exists in an unavailable form [40].

**Table 2.** Molecular ratios and concentrations of the concerned elements of biogas residue (BR) and biogas residue-derived biochar (BRB).

| Sample | C (%) | H (%) | N (%) | S (%) | O (%) | H/C  | C/N   |
|--------|-------|-------|-------|-------|-------|------|-------|
| BR     | 20.34 | 3.32  | 2.41  | 0.84  | 28.48 | 1.95 | 10.59 |
| BRB400 | 19.81 | 1.51  | 1.41  | 0.99  | 21.73 | 0.92 | 17.55 |
| BRB500 | 14.34 | 0.60  | 0.68  | 1.23  | 21.59 | 0.50 | 26.38 |
| BRB600 | 13.95 | 0.41  | 0.58  | 1.41  | 21.21 | 0.35 | 30.11 |
| BRB700 | 13.17 | 0.32  | 0.38  | 1.37  | 19.09 | 0.29 | 43.38 |
| BRB800 | 9.70  | 0.30  | 0.19  | 1.26  | 14.63 | 0.37 | 64.12 |
| BRB900 | 7.07  | 0.63  | 0.14  | 1.57  | 4.925 | 1.07 | 63.33 |

Note: numbers following BRB refer to pyrolysis temperatures.

To characterize the relationship between BR pyrolysis temperature and the degree of aromaticity and hydrophobicity of the biochars, the molecular values of carbon, hydrogen, nitrogen and oxygen

were evaluated. The C/N values not only affect the characteristics of the biochar, but may also influence the levels of C and N during mineralization [41]. After that, given the high values of C/N for biochar, it is possible that N immobilization occurs [42], decreasing the N loss from the soil. The C/N increased from 17.55% at 400 °C to 63.33% at 900 °C. The values of C/N were higher in biochar, from 65.7% to 49.8%, than in their feedstock (BR). This indicated that the loss of nitrogen from the soil could be reduced at higher pyrolysis temperatures. The H/C values were associated with the grade of carbonization. Table 2 shows that the H/C of biochar decreased with increasing pyrolytic temperature. This reflected the increasing degree of structural modification due to the carbonization reactions of biochar with increasing temperature. The lowest H/C value (0.29) at 700 °C suggests that the biochar is highly carbonized. The decrease of H/C values with increasing pyrolysis temperature is consistent with the results from Kloss et al. [43], who found a reduced H/C ratio between 0.7 and 1.0 at 400 °C for poplar-derived biochar. Keiluweit et al. [32] also found a reduction of the H/C ratio from 1.59 to 0.52 for ponderosa pine-derived biochars, and from 1.81 to 0.48 for straw-derived biochars.

### 3.6. Phosphorus Adsorption and Soil Amendment

#### 3.6.1. Adsorption Kinetics

Adsorption kinetics are an important characteristic for defining the efficiency of adsorption [18]. Figure 2a shows the adsorption capacity of phosphorus versus time at an initial concentration of  $10.6 \text{ mg}\cdot\text{L}^{-1}$ . At the initial stage of the process, the adsorption rate was very high, then exhibited a gradual decrease until the adsorption equilibrium was reached. From this characterization of adsorption kinetics, P was initially adsorbed onto the exterior surface of the biochar, then diffused into the pores and adsorbed on the interior surface. Figure 2a indicates that the P adsorption equilibrium of biochar was reached after 24 h, which is consistent with the findings for other kinds of biochar documented by other researchers [14,44], who looked at synthesizing biochar through anaerobic digested sugar beet tailings or tomato leaves and gained P adsorption equilibrium after 24 h. Pyrolysis temperature had a pronounced effect on the biochar properties. The amount of P adsorption ranged from  $23.04 \text{ mg}\cdot\text{g}^{-1}$  of BRB400 to  $70.90 \text{ mg}\cdot\text{g}^{-1}$  of BRB900 (Figure 2b). Therefore, the amount of P adsorbed onto BRB900 was higher compared to other kinds of biochar, demonstrating its refined P adsorption efficiency.

The adsorption kinetics of P on BRB900 were evaluated using the pseudo-first-order model and the pseudo-second-order model, shown in Equations (3) and (4), respectively. The results from the plots in Figure 2c,d show that the correlation coefficient ( $R^2$ ) of the pseudo-second-order kinetic model was higher than that of the pseudo-first-order model, suggesting that the kinetics of P adsorption on BRB could be described better by the pseudo-second-order equation. Figure 2c,d shows that the P adsorption ability of the biochar was  $12.2820 \text{ mg}\cdot\text{g}^{-1}$ . Therefore, the amount of P adsorbed onto BRB900 was greater than that of the traditional biochar. Yao et al. [45] documented the rehabilitation of 13 types of biochar on P adsorption, reporting that the biochars did not show a P adsorption ability. In accordance with the above analysis and FTIR results, the P adsorption capacity in our study may have been due to the oxygen-containing surface groups on the BRB (Figure 1).

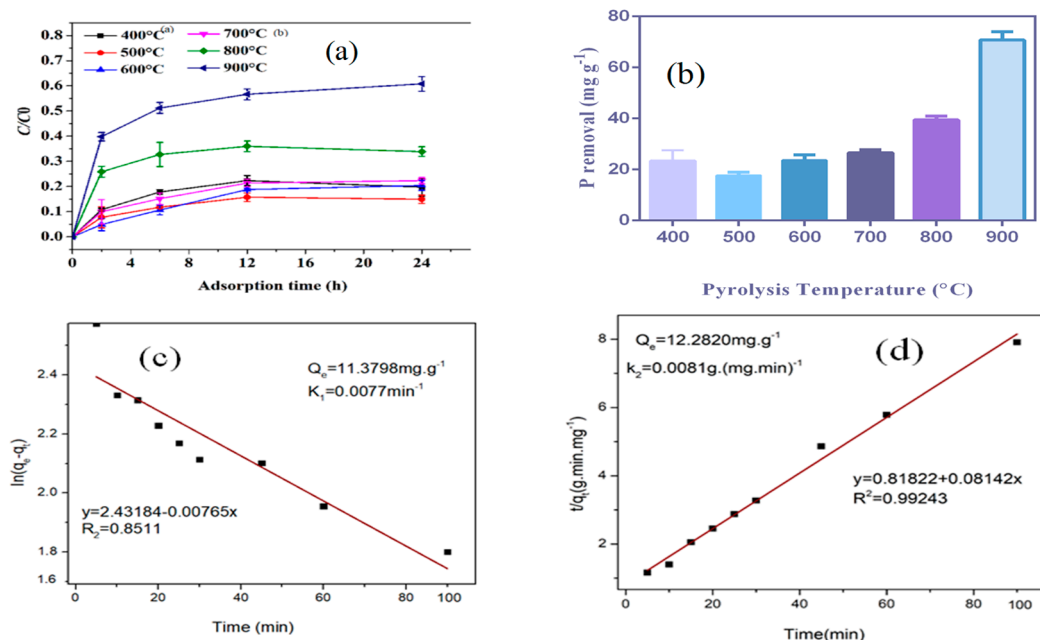


**Figure 2.** Adsorption characteristics of phosphorus on biochar: (a) Variation of adsorption capacity with adsorption time; (b) effect of pyrolysis temperature on phosphorus removal; (c) pseudo-first-order kinetic and (d) pseudo-second-order kinetic models for phosphorus adsorption onto BRB900.

### 3.6.2. Soil Amendment

The effect of BRB at different pyrolysis temperatures on the development of vegetables was examined using pot experiments. Figure 3a shows that *Brassica chinensis* L. had great performance and produced greenish and maximum foliage in pots with BRB600 compared to other treatments and control.

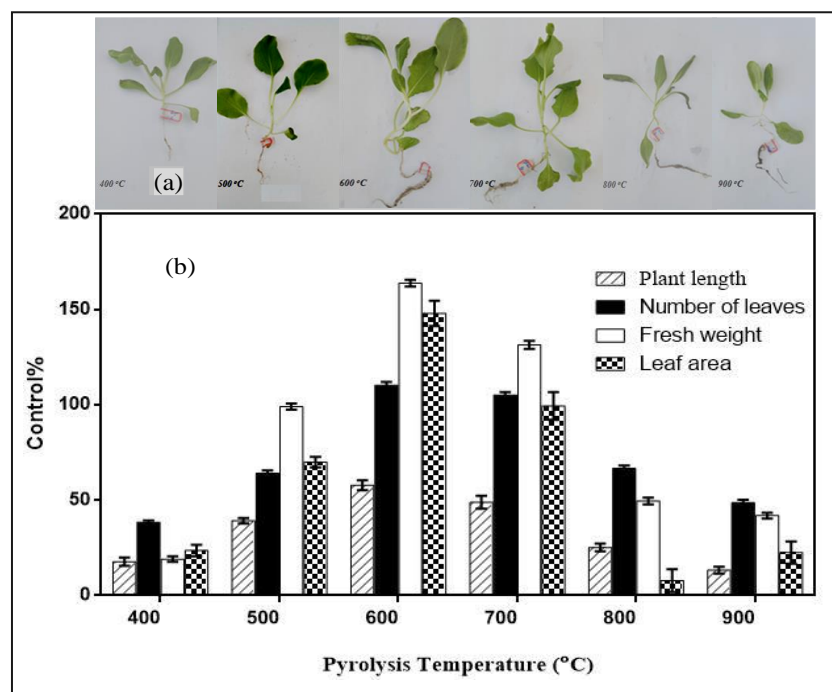


**Figure 3.** Effect of BRB produced under different pyrolysis temperatures on the growth of vegetables: (a) Photograph of plant growth; (b) morphological indices of *Brassica chinensis* L.

The plants grown with BRB600 produced wider leaf blades with dark greenish color (Figure 3b). Adding BRB600 increased plant length, the number of leaves, fresh weight, and the leaf area by 57.78%, 110.26%, 163.81%, and 147.94%, respectively, over the nonamended control (CK). This finding indicates that BRB600 has the best potential to improve the growth of vegetables. Biochar was used to ameliorate the growth of vegetation. The basic principle is that biochar affects plant growth and alters the nutrient levels and water accessibility in soil. The proliferous aspect of biochar can improve the water retention capacity of the soil and simultaneously hold soluble nutrients in the soil. In this study, BRB showed various features (e.g., nutrient content, pH, and capacity to adsorb P) after being subjected to pyrolysis temperatures. BRB600 exhibited the best amelioration in the production of vegetables. Further research regarding the assessment of BRB's effect on plant growth and field-scale experiments should be conducted.

#### 4. Conclusions

In conclusion, assessment of the physicochemical properties of biochar and initial identification of phosphate adsorption and soil amendment show that solid residues from the anaerobic assimilation of food waste for biogas arrangement can be reasonably changed into biochar and could be promoted for phosphorus reclamation for agronomical purposes. The pyrolysis temperature influences the physicochemical properties of the biochar. With high temperatures, the yield and volatile matter decreased and the pH, EC and BET surface area increased. The results from phosphorus adsorption indicate a pronounced effect of pyrolysis temperature on the P adsorption of biochar. The amount of P adsorption increased from  $23.04 \text{ mg}\cdot\text{g}^{-1}$  for BRB400 to  $70.90 \text{ mg}\cdot\text{g}^{-1}$  for BRB900. The amount of P adsorbed onto BRB900 was greater than that of other kinds of biochar. The kinetics of P adsorption on BRB could be solved using the pseudo-second-order equation. The P adsorption capacity of BRB900 was  $12.28 \text{ mg}\cdot\text{g}^{-1}$ , which was larger than that of other traditional biochars. The pot study revealed that biochar is useful for the development of cabbage. The results of this research are important for the design and development of food waste biogas residue-derived biochar. Overall, turning solid residue from the anaerobic digestion residues of food waste for biogas production into biochar for phosphorus recovery and soil amendment applications has potential as a means of solving disposal problems, while creating new markets for food waste biogas residues.

**Author Contributions:** Conceptualization, G.S. and S.A.; Methodology, S.A.; Investigation, S.A., Data curation, S.A. and S.Q.; Writing—original draft, S.A., Resource, Y.H., J.W., H.Z., and W.C.; Writing—review and editing, G.S.

**Funding:** The work was supported by the National Key Research and Development Program of China (grant no. 2018YFD0800205) and the National Natural Science Foundation of China (NSFC 21876109, 21477075).

**Conflicts of Interest:** The authors declare no conflict of interest.

#### References

1. Zhang, C.; Su, H.; Baeyens, J.; Tan, T. Reviewing the anaerobic digestion of food waste for biogas production. *Renew. Sustain. Energy Rev.* **2014**, *38*, 383–392. [[CrossRef](#)]
2. Marcello, P. Does food sharing lead to food waste reduction? An experimental analysis to assess challenges and opportunities of a new consumption model. *J. Clean. Prod.* **2018**, *185*, 749–760.
3. Aschemann-Witzel, J.; de Hooge, I.; Amani, P.; Bech-Larsen, T.; Oostindjer, M. Consumer-related food waste: Causes and potential for action. *Sustainability* **2015**, *7*, 6457–6477. [[CrossRef](#)]
4. Michelini, L.; Principato, L.; Iasevoli, G. Understanding food sharing models to tackle sustainability challenges. *Ecol. Econ.* **2018**, *145*, 205–217. [[CrossRef](#)]
5. Morone, P.; Falcone, P.M.; Lopolito, A. How to promote a new and sustainable food consumption model: A fuzzy cognitive map study. *J. Clean. Prod.* **2019**, *208*, 563–574. [[CrossRef](#)]
6. Gupta, S.; Kua, H.W.; Koh, H.J. Application of biochar from food and wood waste as green admixture for cement mortar. *Sci. Total Environ.* **2018**, *619*, 419–435. [[CrossRef](#)] [[PubMed](#)]
7. Hung, C.-Y.; Tsai, W.-T.; Chen, J.-W.; Lin, Y.-Q.; Chang, Y.-M. Characterization of biochar prepared from biogas digestate. *Waste Manag.* **2017**, *66*, 53–60. [[CrossRef](#)]

8. Stefaniuk, M.; Oleszczuk, P. Characterization of biochars produced from residues from biogas production. *J. Anal. Appl. Pyrolysis* **2015**, *115*, 157–165. [[CrossRef](#)]
9. Pituello, C.; Francioso, O.; Simonetti, G.; Pisi, A.; Torreggiani, A.; Berti, A.; Morari, F. Characterization of chemical–physical, structural and morphological properties of biochars from biowastes produced at different temperatures. *J. Soils Sediments* **2015**, *15*, 792–804. [[CrossRef](#)]
10. Hossain, A.; Serrano, C.; Brammer, J.; Omran, A.; Ahmed, F.; Smith, D.; Davies, P. Combustion of fuel blends containing digestate pyrolysis oil in a multi-cylinder compression ignition engine. *Fuel* **2016**, *171*, 18–28. [[CrossRef](#)]
11. Li, Q.; Xu, M.; Wang, G.; Chen, R.; Qiao, W.; Wang, X. Biochar assisted thermophilic co-digestion of food waste and waste activated sludge under high feedstock to seed sludge ratio in batch experiment. *Bioresour. Technol.* **2018**, *249*, 1009–1016. [[CrossRef](#)] [[PubMed](#)]
12. He, X.; Liu, Z.; Niu, W.; Yang, L.; Zhou, T.; Qin, D.; Niu, Z.; Yuan, Q. Effects of pyrolysis temperature on the physicochemical properties of gas and biochar obtained from pyrolysis of crop residues. *Energy* **2018**, *143*, 746–756. [[CrossRef](#)]
13. López-Cano, I.; Cayuela, M.; Mondini, C.; Takaya, C.; Ross, A.; Sánchez-Monedero, M. Suitability of different agricultural and urban organic wastes as feedstocks for the production of biochar—Part 1: Physicochemical characterisation. *Sustainability* **2018**, *10*, 2265. [[CrossRef](#)]
14. Yao, Y.; Gao, B.; Inyang, M.; Zimmerman, A.R.; Cao, X.; Pullammanappallil, P.; Yang, L. Biochar derived from anaerobically digested sugar beet tailings: Characterization and phosphate removal potential. *Bioresour. Technol.* **2011**, *102*, 6273–6278. [[CrossRef](#)] [[PubMed](#)]
15. Qin, J.; Chen, Q.; Sun, M.; Sun, P.; Shen, G. Pyrolysis temperature-induced changes in the catalytic characteristics of rice husk-derived biochar during 1, 3-dichloropropene degradation. *Chem. Eng. J.* **2017**, *330*, 804–812. [[CrossRef](#)]
16. Inyang, M.; Gao, B.; Pullammanappallil, P.; Ding, W.; Zimmerman, A.R. Biochar from anaerobically digested sugarcane bagasse. *Bioresour. Technol.* **2010**, *101*, 8868–8872. [[CrossRef](#)]
17. Troy, S.M.; Nolan, T.; Leahy, J.J.; Lawlor, P.G.; Healy, M.G.; Kwapinski, W. Effect of sawdust addition and composting of feedstock on renewable energy and biochar production from pyrolysis of anaerobically digested pig manure. *Biomass Bioenergy* **2013**, *49*, 1–9. [[CrossRef](#)]
18. Chen, Q.; Qin, J.; Sun, P.; Cheng, Z.; Shen, G. Cow dung-derived engineered biochar for reclaiming phosphate from aqueous solution and its validation as slow-release fertilizer in soil-crop system. *J. Clean. Prod.* **2018**, *172*, 2009–2018. [[CrossRef](#)]
19. Chen, B.; Chen, Z.; Lv, S. A novel magnetic biochar efficiently sorbs organic pollutants and phosphate. *Bioresour. Technol.* **2011**, *102*, 716–723. [[CrossRef](#)]
20. Hammer, E.C.; Balogh-Brunstad, Z.; Jakobsen, I.; Olsson, P.A.; Stipp, S.L.; Rillig, M.C. A mycorrhizal fungus grows on biochar and captures phosphorus from its surfaces. *Soil Biol. Biochem.* **2014**, *77*, 252–260. [[CrossRef](#)]
21. Chen, L.; Chen, Q.; Rao, P.; Yan, L.; Shakib, A.; Shen, G. Formulating and optimizing a novel biochar-based fertilizer for simultaneous slow-release of nitrogen and immobilization of cadmium. *Sustainability* **2018**, *10*, 2740. [[CrossRef](#)]
22. Collins, L.W.; Chalk, S.J.; Kingston, H.S. Atmospheric pressure microwave sample preparation procedure for the combined analysis of total phosphorus and kjeldahl nitrogen. *Anal. Chem.* **1996**, *68*, 2610–2614. [[CrossRef](#)] [[PubMed](#)]
23. Zhou, K.; Wu, B.; Su, L.; Gao, X.; Chai, X.; Dai, X. Development of nano-CaO<sub>2</sub>-coated clinoptilolite for enhanced phosphorus adsorption and simultaneous removal of cod and nitrogen from sewage. *Chem. Eng. J.* **2017**, *328*, 35–43. [[CrossRef](#)]
24. Yan, J.; Jiang, T.; Yao, Y.; Wang, J.; Cai, Y.; Green, N.W.; Wei, S. Underestimation of phosphorus fraction change in the supernatant after phosphorus adsorption onto iron oxides and iron oxide-natural organic matter complexes. *J. Environ. Sci.* **2017**, *55*, 197–205. [[CrossRef](#)] [[PubMed](#)]
25. Takaya, C.A.; Fletcher, L.A.; Singh, S.; Anyikude, K.U.; Ross, A.B. Phosphate and ammonium sorption capacity of biochar and hydrochar from different wastes. *Chemosphere* **2016**, *145*, 518–527. [[CrossRef](#)] [[PubMed](#)]
26. Belevi, H.; Moench, H. Factors determining the element behavior in municipal solid waste incinerators. 1. Field studies. *Environ. Sci. Technol.* **2000**, *34*, 2501–2506. [[CrossRef](#)]

27. Thangalazhy-Gopakumar, S.; Adhikari, S.; Ravindran, H.; Gupta, R.B.; Fasina, O.; Tu, M.; Fernando, S.D. Physiochemical properties of bio-oil produced at various temperatures from pine wood using an auger reactor. *Bioresour. Technol.* **2010**, *101*, 8389–8395. [[CrossRef](#)]
28. DeSisto, W.J.; Hill, N.; Beis, S.H.; Mukkamala, S.; Joseph, J.; Baker, C.; Ong, T.-H.; Stemmler, E.A.; Wheeler, M.C.; Frederick, B.G. Fast pyrolysis of pine sawdust in a fluidized-bed reactor. *Energy Fuels* **2010**, *24*, 2642–2651. [[CrossRef](#)]
29. Cao, X.; Harris, W. Properties of dairy-manure-derived biochar pertinent to its potential use in remediation. *Bioresour. Technol.* **2010**, *101*, 5222–5228. [[CrossRef](#)]
30. del Martínez-Ballesta, M.C.; Silva, C.; Lopez-Berenguer, C.; Cabañero, F.; Carvajal, M. Plant aquaporins: New perspectives on water and nutrient uptake in saline environment. *Plant Biol.* **2006**, *8*, 535–546. [[CrossRef](#)]
31. Al-Wabel, M.I.; Al-Omran, A.; El-Naggar, A.H.; Nadeem, M.; Usman, A.R. Pyrolysis temperature induced changes in characteristics and chemical composition of biochar produced from *conocarpus* wastes. *Bioresour. Technol.* **2013**, *131*, 374–379. [[CrossRef](#)] [[PubMed](#)]
32. Keiluweit, M.; Nico, P.S.; Johnson, M.G.; Kleber, M. Dynamic molecular structure of plant biomass-derived black carbon (biochar). *Environ. Sci. Technol.* **2010**, *44*, 1247–1253. [[CrossRef](#)]
33. Mukome, F.N.; Parikh, S.J. Chemical, physical, and surface characterization of biochar. In *Biochar: Production, Characterization, and Applications*; Ok, Y.S., Uchimiya, S.M., Chang, S.X., Bolan, N., Eds.; CRC Press: Boca Raton, FL, USA, 2015; pp. 68–96.
34. Onorevoli, B.; da Silva Maciel, G.P.; Machado, M.E.; Corbelini, V.; Caramão, E.B.; Jacques, R.A. Characterization of feedstock and biochar from energetic tobacco seed waste pyrolysis and potential application of biochar as an adsorbent. *J. Environ. Chem. Eng.* **2018**, *6*, 1279–1287. [[CrossRef](#)]
35. El Ouqaoudi, F.Z.; El Fels, L.; Lemée, L.; Amblès, A.; Hafidi, M. Evaluation of lignocellulose compost stability and maturity using spectroscopic (ftir) and thermal (tga/tda) analysis. *Ecol. Eng.* **2015**, *75*, 217–222. [[CrossRef](#)]
36. Özsín, G.; Pütün, A.E. Kinetics and evolved gas analysis for pyrolysis of food processing wastes using tga/ms/ft-ir. *Waste Manag.* **2017**, *64*, 315–326. [[CrossRef](#)]
37. Zbytniewski, R.; Buszewski, B. Characterization of natural organic matter (nom) derived from sewage sludge compost. Part 1: Chemical and spectroscopic properties. *Bioresour. Technol.* **2005**, *96*, 471–478. [[CrossRef](#)] [[PubMed](#)]
38. Tandy, S.; Healey, J.R.; Nason, M.A.; Williamson, J.C.; Jones, D.L.; Thain, S.C. Ft-ir as an alternative method for measuring chemical properties during composting. *Bioresour. Technol.* **2010**, *101*, 5431–5436. [[CrossRef](#)]
39. Agrafioti, E.; Bouras, G.; Kalderis, D.; Diamadopoulos, E. Biochar production by sewage sludge pyrolysis. *J. Anal. Appl. Pyrolysis* **2013**, *101*, 72–78. [[CrossRef](#)]
40. Chan, K.; Xu, Z. 2009biochar: Nutrient properties and their enhancement. In *Biochar for Environmental Management: Science and Technology*; Earthscan: London, UK, 2009; p. 6784.
41. Krull, E.S.; Baldock, J.A.; Skjemstad, J.O.; Smernik, R.J. Characteristics of biochar: Organo-chemical properties. In *Biochar for Environmental Management: Science and Technology*; Earthscan: London, UK, 2009.
42. Atkinson, C.J.; Fitzgerald, J.D.; Hipps, N.A. Potential mechanisms for achieving agricultural benefits from biochar application to temperate soils: A review. *Plant Soil* **2010**, *337*, 1–18. [[CrossRef](#)]
43. Kloss, S.; Sass, O.; Geitner, C.; Prietzel, J. Soil properties and charcoal dynamics of burnt soils in the tyrolean limestone alps. *Catena* **2012**, *99*, 75–82. [[CrossRef](#)]
44. Yao, Y.; Gao, B.; Chen, J.; Yang, L. Engineered biochar reclaiming phosphate from aqueous solutions: Mechanisms and potential application as a slow-release fertilizer. *Environ. Sci. Technol.* **2013**, *47*, 8700–8708. [[CrossRef](#)] [[PubMed](#)]
45. Yao, Y.; Gao, B.; Zhang, M.; Inyang, M.; Zimmerman, A.R. Effect of biochar amendment on sorption and leaching of nitrate, ammonium, and phosphate in a sandy soil. *Chemosphere* **2012**, *89*, 1467–1471. [[CrossRef](#)] [[PubMed](#)]

